

Magnonic φ Josephson junctions and synchronized precession

Kouki Nakata,¹ Ji Zou,² Jelena Klinovaja,² and Daniel Loss^{2,3}

¹*Advanced Science Research Center, Japan Atomic Energy Agency, Tokai, Ibaraki 319-1195, Japan*

²*Department of Physics, University of Basel, Klingelbergstrasse 82, 4056 Basel, Switzerland*

³*Center for Emergent Matter Science, RIKEN, 2-1 Hirosawa, Wako-shi, Saitama 351-0198, Japan*

(Dated: August 9, 2024)

There has been a growing interest in non-Hermitian physics. One of its main goals is to engineer dissipation and to explore ensuing functionality. In magnonics, the effect of dissipation due to local damping on magnon transport has been explored. However, the effects of non-local damping on the magnonic analog of the Josephson effect remain missing, despite that non-local damping is inevitable and has been playing a central role in magnonics. Here, we uncover theoretically that a surprisingly rich dynamics can emerge in magnetic junctions due to intrinsic non-local damping, using analytical and numerical methods. In particular, under microwave pumping, we show that coherent spin precession in the right and left insulating ferromagnet (FM) of the junction becomes synchronized by non-local damping and thereby a magnonic analog of the φ Josephson junction emerges, where φ stands here for the relative precession phase of right and left FM in the stationary limit. Remarkably, φ decreases monotonically from π to $\pi/2$ as the magnon-magnon interaction, arising from spin anisotropies, increases. Moreover, we also find a magnonic diode effect giving rise to rectification of magnon currents. Our predictions are readily testable with current device and measurement technologies at room temperatures.

I. INTRODUCTION

Recently, non-Hermitian physics [1] has been attracting growing interest from both fundamental science and applications such as energy-efficient devices. One of its main themes is to engineer dissipation and to explore the resulting functionality. Since magnons are intrinsically damped in magnetic systems, the goal of non-Hermitian physics aligns well with magnonics [2–4], which aims at efficient transmission and processing of information for computing and communication technologies using magnons as its carrier in units of the Bohr magneton μ_B . To this end, establishing methods for the control and manipulation of magnon transport subjected to dissipation is crucial. In magnonics, the effect of dissipation due to local (Gilbert) damping on magnon transport, such as the magnonic analog of the Josephson effect [5], has been explored [6–8], where the macroscopic coherent magnon state, the key ingredient for the magnonic Josephson effect, realizes an oscillating behavior of magnon transport. However, the effect of non-local damping on the magnonic Josephson effect and the resulting functionality remain missing, despite that non-local damping is inevitable and has been playing a central role in non-Hermitian magnonics [9–11].

Here, we fill this gap. We find that the inherent non-local damping leads to rich dynamics, and, interestingly, can be utilized to realize a magnonic analog of the φ Josephson junction [12–31] [32]. Under microwave pumping, coherent spin precession in each insulating ferromagnet (FM) of the magnetic junction (see Fig. 1) is synchronized by non-local damping as time advances and gives rise of a magnonic φ Josephson junction, where φ stands for the stationary value of the relative precession phase of the left and right FMs. Interestingly, we find that φ decreases monotonically from π to $\pi/2$ as the magnon-

magnon interaction, arising from spin anisotropies across the junction, increases. Applying microwaves to each FM continuously, the junction reaches the nonequilibrium steady state where the loss of magnons due to dissipation is precisely balanced by the injection of magnons.

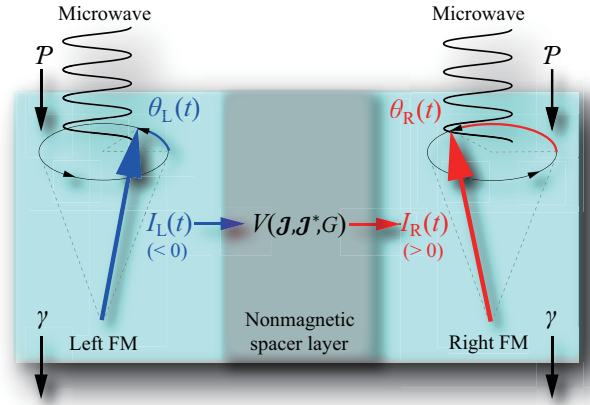


FIG. 1. Magnonic φ Josephson junction, formed by a ferromagnetic bilayer coupled by a non-magnetic spacer. Magnons are subjected to local damping at rate $\gamma > 0$. The spacer layer-mediated interaction V between the two FMs consists of coherent coupling (\mathcal{J}) and non-local damping (G). Under microwave pumping, the spatially uniform mode of magnons is injected into each FM at rate \mathcal{P} , generating coherent spin precessions. The loss of magnons due to dissipation is exactly balanced by the injection of magnons. In the steady state, the spin precessions in each FM get synchronized due to non-local damping and a relative precession angle emerges $\varphi = \lim_{t \rightarrow \infty} [\theta_R(t) - \theta_L(t)]$ that depends on the magnon-magnon interaction. The associated magnon currents $I_{L,R}$ get rectified when $G \neq 0$.

Hence, spins in each FM continue to precess coherently, and the synchronized precession of the left and the right magnetization remains stable even at room temperature. Finally, we show that the magnetic junction exhibits rectification and acts as a diode for the magnon current.

This paper is organized as follows. In Sec. II, we introduce the model system for coherent magnons under microwave pumping, magnonic Josephson junction, and derive the magnonic Josephson equations in the presence of non-local damping. We then describe the synchronized precession of the left and the right magnetization in magnonic φ Josephson junctions and study the behavior of φ as a function of magnon-magnon interactions in Sec. III. We also show that magnonic φ Josephson junctions exhibit a rectification due to non-local damping in Sec. IV. In Sec. V, we discuss experimental feasibility of our theoretical predictions. Finally, we summarize and give some conclusions in Sec. VI. Technical details are deferred to the Appendices.

II. MAGNONIC JOSEPHSON JUNCTIONS

We consider a magnetic junction, shown in Fig. 1, consisting of a bilayer of two insulating ferromagnetic layers, where the two FMs are separated by a nonmagnetic spacer layer, thereby weakly spin-exchange coupled. Applying microwaves to each FM and tuning the microwave frequency $\Omega > 0$ of GHz to the magnon energy gap, ferromagnetic resonance is generated for each FM separately, where spins precess coherently. Under this microwave pumping, the zero wavenumber mode (i.e., spatially uniform mode) of magnons is excited and injected into each FM at the rate of $\mathcal{P} > 0$ [33]. The magnons are subjected to local Gilbert damping at the rate $\gamma > 0$ in each FM.

In addition, there is non-local damping [9, 10] that is mediated by the spacer interaction between the two FMs, see Fig. 1. Using the Holstein-Primakoff transformation [34], this coupling term becomes to leading order [11] $V = (\mathcal{J} - i\hbar G/2)a_L^\dagger a_R + (\mathcal{J}^* - i\hbar G/2)a_L a_R^\dagger$, where $a_{L(R)}^{(\dagger)}$ represents the magnon annihilation (creation) op-

erator for the zero wavenumber mode, which satisfies the bosonic commutation relation. Here, $\mathcal{J} \in \mathbb{C}$, with its complex conjugate \mathcal{J}^* , describes coherent coupling, while $\hbar G \in \mathbb{R}$ describes the non-local damping (or dissipative coupling) [11]. The real part of coherent coupling, $\text{Re}(\mathcal{J}) = \mathcal{J}_{\text{Re}}$, arises from the symmetric spin-exchange interaction between the two FMs, while its imaginary part [5, 33, 35, 36], $\text{Im}(\mathcal{J}) = \mathcal{J}_{\text{Im}}$, is induced, for example, by the Dzyaloshinskii-Moriya interaction when the spatial inversion symmetry of the nonmagnetic spacer layer is broken [37]. Each component of \mathcal{J}/\hbar can reach MHz in experiments [38, 39]. The values of γ and G are typically within the MHz regime [40], and the condition, $\hbar\Omega \gg |\mathcal{J}|, \hbar\gamma, |\hbar G|$, is satisfied. The condition $|G| \leq 2\gamma$ ensures the complete positivity of the system dynamics [11, 41, 42], and we focus on this regime henceforth. We note that the coupling term V becomes non-Hermitian due to non-local damping, i.e., $V \neq V^\dagger$ for $G \neq 0$.

The magnon-magnon interaction in the left (right) FM, $U_{L(R)}$, arises from anisotropies of spin, where $U_L = (U/2)a_L^\dagger a_L^\dagger a_L a_L$, $U_R = (U/2)a_R^\dagger a_R^\dagger a_R a_R$. Here, U can take both positive and negative values, depending on the combination of anisotropies such as the spin anisotropy along the quantization axis and the anisotropy of the spin-exchange interaction in each FM [5, 33].

In this study, we envisage to continuously apply microwaves to each FM, which results in spins exhibiting macroscopic coherent precession characterized as $\langle a_{L(R)}(t) \rangle \neq 0$ [33]. Therefore, assuming a macroscopic coherent magnon state, thereby using the semiclassical approximation, we replace the operators $a_L(t)$ and $a_R(t)$ by their expectation values as $\langle a_L(t) \rangle = \sqrt{N_L(t)}e^{i\theta_L(t)}$ and $\langle a_R(t) \rangle = \sqrt{N_R(t)}e^{i\theta_R(t)}$, respectively, where $N_{L(R)}(t) > 0$ represents the number of coherent magnons for each site in the left (right) FM and $\theta_{L(R)}$ is the phase (see Fig. 1). Defining the relative precession phase as $\theta(t) = \theta_R(t) - \theta_L(t)$, each time evolution [e.g., $\dot{\theta}(t)$ represents the time derivative of $\theta(t)$] is described as (see the Appendices for details [43])

$$\dot{\theta}(t) = \frac{\mathcal{J}_{\text{Re}}}{\hbar} \cos \theta(t) \left(\sqrt{\frac{N_R(t)}{N_L(t)}} - \sqrt{\frac{N_L(t)}{N_R(t)}} \right) + \sin \theta(t) \left[\left(\frac{\mathcal{J}_{\text{Im}}}{\hbar} + \frac{G}{2} \right) \sqrt{\frac{N_L(t)}{N_R(t)}} - \left(\frac{\mathcal{J}_{\text{Im}}}{\hbar} - \frac{G}{2} \right) \sqrt{\frac{N_R(t)}{N_L(t)}} \right] + u[N_L(t) - N_R(t)], \quad (1a)$$

$$\dot{N}_{L/R}(t) = -2\gamma N_{L/R}(t) \pm 2 \left[\frac{\mathcal{J}_{\text{Re}}}{\hbar} \sin \theta(t) + \left(\frac{\mathcal{J}_{\text{Im}}}{\hbar} \mp \frac{G}{2} \right) \cos \theta(t) \right] \sqrt{N_L(t)N_R(t)} + \mathcal{P}, \quad (1b)$$

where $u = U/\hbar$. The second term on the right-hand side of Eq. (1b) describes the nonmagnetic spacer layer-mediated transport of coherent magnons in the junction.

The transport of coherent magnons in this junction

is analogous to the Josephson effect [44] in the sense that the current arises as the term of the order of V , $O(V)$, for the interaction $V = V(\mathcal{J}, \mathcal{J}^*, G)$ between the two FMs (see Fig. 1) and is characterized by the rel-

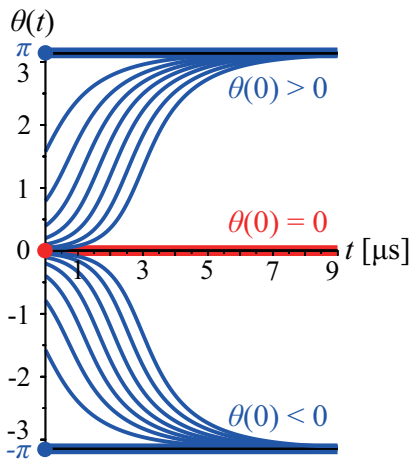


FIG. 2. Plots of the relative phase $\theta(t)$ as a function of time in the absence of the magnon-magnon interaction, i.e., $u = 0$, for the initial condition $\theta(0) = 0$ and $|\theta(0)| = \pi/2^n$ with $n = 0, 1, \dots, 7$ obtained by numerically solving Eqs. (3a)-(3c) for the parameter values $\mathcal{J}_{\text{Re}} = 0$, $\mathcal{J}_{\text{Im}}/\hbar = G/2 = 0.5$ MHz, $\gamma = 1.1$ MHz, $\mathcal{P} = 2\gamma = 2.2$ MHz, and $N_L(0) = N_R(0) = 10^{-6}$. As time advances, coherent spin precession in each FM is synchronized and forms the magnonic π Josephson junction as $\varphi = \theta(t \rightarrow \infty) = \pm\pi$ for $\theta(0) \neq 0$. The initial condition $\theta(0) = 0$ for $u = 0$ results in $\varphi = 0$.

ative precession phase $\theta(t)$. For these reasons [37], we refer to the transport of coherent magnons and the junction as the magnonic Josephson effect and the magnonic Josephson junction, respectively. Note that, in contrast, the current for incoherent magnons arises from a term of $O(V^2)$ [45, 46].

III. SYNCHRONIZED PRECESSION

To seek for a junction setup that exhibits synchronization and rectification effects, we consider the case where

$$\mathcal{J}_{\text{Re}} = 0 \quad \text{and} \quad \mathcal{J}_{\text{Im}}/\hbar = G/2 > 0. \quad (2)$$

Under these assumptions, Eqs. (1a)-(1b) become

$$\dot{\theta}(t) = G\sqrt{N_L/N_R} \sin \theta + u(N_L - N_R), \quad (3a)$$

$$\dot{N}_L = -2\gamma N_L + \mathcal{P}, \quad (3b)$$

$$\dot{N}_R = -2\gamma N_R - 2G\sqrt{N_L N_R} \cos \theta + \mathcal{P}, \quad (3c)$$

where we suppressed for brevity the explicit time-dependence of the quantities $\theta(t)$ and $N_{L/R}(t)$. Under microwave pumping \mathcal{P} , the nonequilibrium steady state $\dot{\theta}(t) = \dot{N}_L(t) = \dot{N}_R(t) = 0$ is realized, where $\theta(t)$, $N_L(t)$, and $N_R(t)$ approach their stationary values as time advances, i.e., $\varphi = \theta(t \rightarrow \infty)$ and $N_{L(R)}(t \rightarrow \infty) = N_{L(R)}^\infty$. Using Eqs. (3a)-(3c), we find the following relations be-

tween these asymptotic quantities:

$$\cos \varphi = (\gamma/G)(N_L^\infty - N_R^\infty)/\sqrt{N_R^\infty N_L^\infty}, \quad (4a)$$

$$\tan \varphi = -uN_R^\infty/\gamma, \quad (4b)$$

where $N_L^\infty = \mathcal{P}/2\gamma$ is a constant, while N_R^∞ becomes a function of the relative precession phase φ . In what follows, we will show that there is a unique solution to the system of Eqs. (4a) and (4b). Thereby, a magnonic analog of the φ Josephson junction [12–31] is realized.

A. Absence of magnon interaction: $u = 0$

First, we study the behavior of φ in the absence of the magnon-magnon interaction, $u = 0$. From Eq. (4b), we immediately find that φ can only be equal to $\pm\pi$ or 0. One of these three values is chosen based on the initial condition $\theta(0)$. Figure 2 shows the plots of the relative phase $\theta(t)$ for several initial conditions $\theta(0)$ as a function of time obtained by numerically solving Eqs. (3a)-(3c). If $\theta(0) = 0$, the relative phase stays constant, $\theta(t) = 0$. If the symmetry is broken, i.e., $\theta(0) \neq 0$, we have $\varphi = \pi \operatorname{sgn} \theta(0)$. This shows that the coherent spin precessions in each FM get synchronized with each other as time advances. This asymptotic locking of the spin precessions is a direct consequence of the dissipative coupling term G . The junction behavior represents a magnonic analog of the well-known π Josephson junction effect in superconductors [12–17].

Figure 2 also shows that the point $\theta(0) = 0$ is unstable in the sense that $\varphi = 0$ for the initial condition $\theta(0) = 0$, whereas $\varphi = \pm\pi$ for $\theta(0) \neq 0$. However, to realize such a special condition, $\theta(0) = 0$ with $u = 0$, will be out of experimental reach. Moreover, in what follows, we will show that any finite value of u results in $\varphi \neq 0$, no matter what initial value we choose for $\theta(0)$ including the fine-tuned value $\theta(0) = 0$, see Fig. 3.

We emphasize that our results are independent of the initial values $N_L(0)$ and $N_R(0)$ and do not depend on the assumption that both FMs are pumped at the same rate \mathcal{P} . A detailed discussion is available in the Appendices [43]. We also remark that the synchronized precession of the left and the right magnetization, $\dot{\theta}(t) = 0$, remains valid even if the parameter values deviate from Eq. (2). For details of the parameter dependence of our results, see the Appendices [43], where we numerically show the robustness of the synchronized precession. We note that under the initial condition $\theta(0) = 0$, we have $\varphi \neq 0$ for $\mathcal{J}_{\text{Re}} \neq 0$, whereas $\varphi = 0$ for $\mathcal{J}_{\text{Re}} = 0$. Also in this sense, the point $\theta(0) = 0$ is unstable. See the Appendices [43] for more details.

B. Finite magnon interaction: $u \neq 0$

Next, we study the behavior of φ in the presence of the magnon-magnon interaction, $u \neq 0$, and determine φ as a

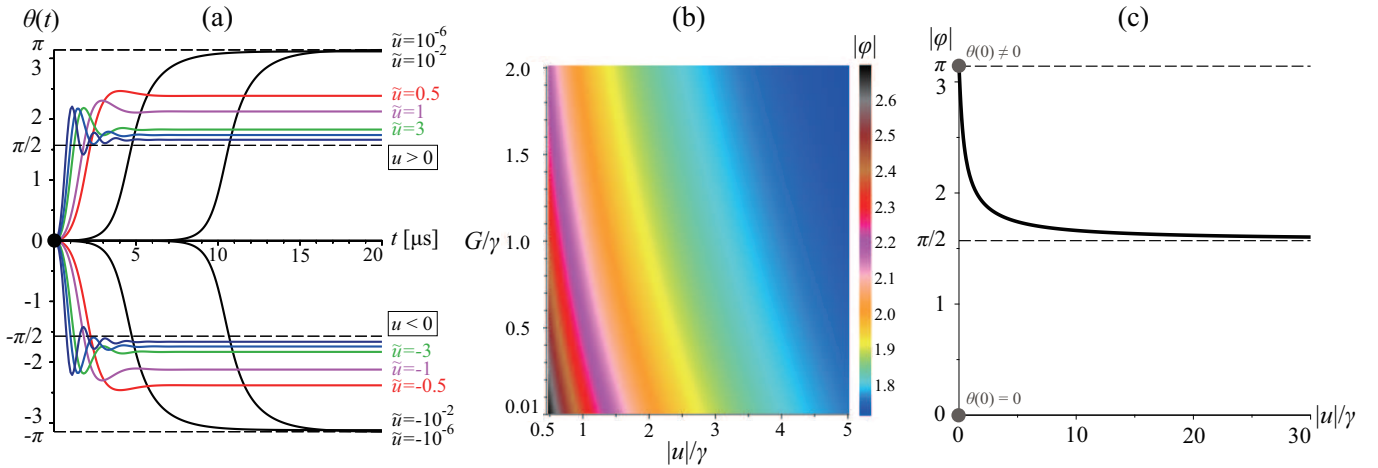


FIG. 3. (a) Plots of the relative phase $\theta(t)$ as a function of time for several values of \tilde{u} obtained by numerically solving Eqs. (3a)-(3c) for the same parameter values as in Fig. 2 as well as for $\theta(0) = 0$. The stationary relative phase, $\varphi = \theta(t \rightarrow \infty)$, decreases from $|\varphi| = \pi$ to $|\varphi| = \pi/2$ as the magnon-magnon interaction $|\tilde{u}|$ increases, where we set $|\tilde{u}| = 10^{-6}, 10^{-2}, 0.5, 1, 3, 5, 10$. We note that $\text{sgn}(\varphi) = \text{sgn}(u)$. (b,c) The relative phase $|\varphi|$ decreases as $|u|/\gamma$ and G/γ increase. These plots are obtained by numerically solving Eq. (5) for the same parameter values as in Fig. 3(a). (c) Plot of $|\varphi|$ as a function of $|u|/\gamma$, showing that $|\varphi|$ decreases monotonically from π to $\pi/2$ as $|u|/\gamma$ increases. For $u \neq 0$, the value of $|\varphi|$ does not depend on the initial conditions. For $u = 0$, $|\varphi|$ depends on the initial condition $\theta(0)$ as $|\varphi| = \pi$ for $\theta(0) \neq 0$, whereas $\varphi = 0$ for $\theta(0) = 0$ (see Fig. 2).

function of u . First, from Eq. (4b), we deduce that $\varphi(u)$ is an odd function of u , i.e., $\varphi(u) = -\varphi(-u) \pmod{2\pi}$. Here, we used that $N_R^\infty(\varphi) = N_R^\infty(-\varphi)$, which follows from Eq. (4a). In Fig. 3, we solve numerically Eqs. (3a)-(3c) and confirm that $\varphi(u)$ is odd. Remarkably, even if the initial condition is chosen as $\theta(0) = 0$, for $u \neq 0$, the magnitude of φ monotonically decreases from $|\varphi| = \pi$ to $|\varphi| = \pi/2$ as the magnitude of the magnon-magnon interaction increases. We note that this condition is consistent with the requirement that the direction of magnon propagation in the junction, see Fig. 1, is chosen to be from left to right (see also below).

Introducing the rescaled magnon-magnon interaction $\tilde{u} = (u/\gamma)N_L^\infty$ and combining Eqs. (3a)-(3c), we get the following implicit equation on $\tan \varphi$:

$$\tan^4 \varphi + 2\tilde{u} \tan^3 \varphi + (1 + \tilde{u}^2) \tan^2 \varphi + \left[2 + (G/\gamma)^2 \right] \tilde{u} \tan \varphi + \tilde{u}^2 = 0, \quad (5)$$

whose solution gives us φ as function of \tilde{u} . For $\varphi \in [-\pi, \pi]$, there are generally four solutions for φ . The two solutions with $\cos \varphi > 0$ are excluded as they will result in an unphysical direction of the current I_R that is set by the nonlocal interaction term V (see below). Finally, one more solution is eliminated as it breaks the condition $\tan \varphi < -\tilde{u}$, which follows from Eqs. (4a) and (4b) for $\tilde{u} > 0$. That leaves us with a unique solution for φ .

In Fig. 3(b), we investigate $|\varphi|$ as a function of both $|u|/\gamma$ and G/γ by numerically solving Eq. (5). For a given \tilde{u} (G), $|\varphi|$ decreases monotonically from π to $\pi/2$ as G (\tilde{u}) increases, see Fig. 3(b,c). The asymptotic expressions for φ for the two limiting cases of weak and strong inter-

actions can be obtained also analytically. Indeed, from Eqs. (5) and (4a) and for strong interactions, $\tilde{u} \gg 1$, we get in leading order in $1/\tilde{u}$

$$\varphi \simeq \pi/2 + 1/\tilde{u}, \quad (6a)$$

$$N_R^\infty/N_L^\infty \simeq 1 + G/\tilde{u}\gamma. \quad (6b)$$

In the opposite limit of weak interactions, $0 < \tilde{u} \ll 1$, we obtain, keeping leading corrections in \tilde{u} in each quantity,

$$\varphi \simeq \pi - c\tilde{u}, \quad (7a)$$

$$N_R^\infty/N_L^\infty \simeq c \left(1 - G(c\tilde{u})^2/\sqrt{G^2 + 4\gamma^2} \right) \quad (7b)$$

where $c = (\sqrt{1 + (G/2\gamma)^2} + G/2\gamma)^2$. These equations together with Fig. 3(c) are one of the main results of this study. Remarkably, both limiting values for φ , namely $\pi/2$ and π , are obviously universal, i.e., independent of any material properties as well as of initial conditions. This underlines the robust and universal property of the synchronization of precessions brought about by the nonlocal damping in magnetic junctions driven by microwaves.

IV. RECTIFICATION

The magnonic φ Josephson junction can be regarded as a magnonic analog of the Josephson diode [47–49], in the sense that it exhibits a rectification effect for the magnon currents, as we will show next. From Eq. (1b) one gets that the current of coherent magnons that flows

from the nonmagnetic spacer layer into the left (right) FM (see Fig. 1), $I_{L(R)}(t) = O(V)$, is given by

$$I_{L/R} = \pm 2 \left[\frac{\mathcal{J}_{\text{Re}}}{\hbar} \sin \theta + \left(\frac{\mathcal{J}_{\text{Im}}}{\hbar} \mp \frac{G}{2} \right) \cos \theta \right] \sqrt{N_L N_R}, \quad (8)$$

in units of $g\mu_B$ for the g -factor g of the constituent spins, and where we suppressed for brevity the explicit time-dependence of the quantities $\theta(t)$ and $N_{L/R}(t)$. The condition specified in Eq. (2) results in

$$I_L(t) = 0, \quad (9a)$$

$$I_R(t) = -2G\sqrt{N_L(t)N_R(t)} \cos \theta. \quad (9b)$$

Since the nonequilibrium steady state is realized under microwave pumping \mathcal{P} , the current $I_R(t)$ continues to flow while keeping the rectification effect characterized by $I_L(t) = 0$ in the magnonic φ Josephson junction (see Fig. 1). We emphasize that the rectification of the magnon current holds also in the presence of the magnon-magnon interaction.

Note that our analytical solutions for φ must satisfy $\cos \varphi < 0$ and thus the magnitude of φ is bounded as $\pi/2 < |\varphi| \leq \pi$ to ensure $\lim_{t \rightarrow \infty} I_R(t) \geq 0$. We recall that the non-local damping G provides the non-Hermitian property to the nonmagnetic spacer layer-mediated interaction described by V . Under the special conditions stated in Eq. (2) one gets $V = -i\hbar G a_L a_R^\dagger$. This shows that propagation of magnons becomes chiral and is allowed only in the direction from left to right in the junction. This is consistent with the sign choice of the current and its direction as shown in Fig. 1.

In the absence of non-local damping, $G = 0$, the current of coherent magnons propagates in both directions through the nonmagnetic spacer layer, from the left to the right FM and vice versa [5]. This results in $I_R(t) = -I_L(t)$ for $G = 0$ [see Eqs. (8)]. Thus, we see that rectification only occurs in the presence of non-local damping when $G \neq 0$.

If instead of Eq. (2), one uses the condition

$$\mathcal{J}_{\text{Re}} = 0 \quad \text{and} \quad \mathcal{J}_{\text{Im}}/\hbar = -G/2, \quad (10)$$

we get from Eq. (8) that

$$I_L(t) = -2G\sqrt{N_L(t)N_R(t)} \cos \theta(t), \quad (11a)$$

$$I_R(t) = 0. \quad (11b)$$

Thus, the rectification effect changes its direction. We conclude that the polarity of the rectification effect is determined by the sign of G .

V. EXPERIMENTAL FEASIBILITY

The key ingredient for the magnonic Josephson effect is the coherent magnon state $\langle a_{L(R)}(t) \rangle \neq 0$ (i.e., co-

herent spin precession), and it can be realized through microwave pumping [33]. Since each component of coherent coupling \mathcal{J} is tunable by adjusting the thickness of the nonmagnetic spacer layer [38, 50–53] or applying an electric field [54–57], the magnonic φ Josephson junction is realizable by tuning coherent coupling appropriately. Moreover, applying microwave to each FM continuously, the loss of magnons due to dissipation is precisely balanced by the injection of magnons achieved through microwave pumping. Therefore, spins in each FM continue to precess coherently, and the synchronized precession of the magnonic φ Josephson junctions remains stable. Thus, our theoretical prediction is within experimental reach with current device and measurement techniques through magnetization measurement.

For the observation of our theoretical predictions, a few comments are in order. It has been established in experiments in which one attaches a heavy metal (e.g., platinum) to FMs that magnon currents can be measured electrically by the inverse spin Hall effect [58]. This is a promising way to observe the effects predicted in this work. Here it should be noted that the coherence length of magnons in yttrium iron garnet (YIG) reaches the order of $10 \mu\text{m}$ (i.e., macroscopic) [59, 60], and experimental observation of a magnonic Josephson effect in YIG and that of a magnon supercurrent in YIG have been reported in Refs. [61] and [62], respectively, by using Brillouin light scattering spectroscopy. Hence we expect that YIG is one of the best platforms for the realization of our proposed setup. Note that the magnitude of the non-local damping can be comparable to the local damping in general [40], and recent experimental studies reported that the value of the local damping for YIG reaches the order of MHz [63].

VI. CONCLUSION

We have investigated the effect of non-local damping on magnetic junctions and found that it serves as the key ingredient for the synchronized precession and gives rise to a magnonic φ Josephson junction. The spacer layer-mediated interaction between the two FMs in the junctions consists of coherent coupling and non-local damping, and it becomes non-Hermitian due to non-local damping. Tuning them appropriately, coherent spin precession in each FM is synchronized by non-local damping as time advances and forms a φ Josephson junction, where the relative precession angle φ decreases monotonically from $|\varphi| = \pi$ to $|\varphi| = \pi/2$ as the magnitude of the magnon-magnon interaction increases, with both limiting values being entirely universal. The magnon currents in the junction exhibits rectification and gives rise to a magnonic diode effect. Applying microwaves to each FM continuously, the junction reaches the nonequilibrium steady state where the loss of magnons due to dissipation is precisely balanced by the injection of magnons achieved through microwave pumping. Hence, spins in

each FM continue to precess coherently, and the synchronized precession of the left and the right magnetization remains stable.

ACKNOWLEDGMENTS

This work was supported by the Georg H. Endress Foundation and by the Swiss National Science Foundation, and NCCR SPIN (grant number 51NF40-180604). K.N. acknowledges support by JSPS KAKENHI Grants

No. JP22K03519.

Appendix A: Magnonic Josephson equations

In this Appendix, we provide details on the derivation of the magnonic Josephson equations. The effective non-Hermitian Hamiltonian \mathcal{H} for the magnonic Josephson junction is given as [5, 11, 33] $\mathcal{H} = \mathcal{H}_L + \mathcal{H}_R + V + U_L + U_R$ with (see also main text) $\mathcal{H}_L = \hbar(\Omega - i\gamma)a_L^\dagger a_L$ and $\mathcal{H}_R = \hbar(\Omega - i\gamma)a_R^\dagger a_R$, where $a_{L(R)}^{(\dagger)}$ represents the magnon annihilation (creation) operator for the zero wavenumber mode (i.e., spatially uniform mode) in the left (right) FM. This provides the time evolution of each operator as

$$i\hbar\dot{a}_L(t) = \hbar(\Omega - i\gamma)a_L(t) + (\mathcal{J} - i\hbar G/2)a_R(t) + Ua_L^\dagger(t)a_L(t)a_L(t), \quad (\text{A1a})$$

$$i\hbar\dot{a}_R(t) = \hbar(\Omega - i\gamma)a_R(t) + (\mathcal{J}^* - i\hbar G/2)a_L(t) + Ua_R^\dagger(t)a_R(t)a_R(t). \quad (\text{A1b})$$

Here, assuming a macroscopic coherent magnon state, thereby using the semiclassical approximation, we replace the operators $a_L(t)$ and $a_R(t)$ by their expectation values as $\langle a_L(t) \rangle = \sqrt{N_L(t)}e^{i\theta_L(t)}$ and $\langle a_R(t) \rangle = \sqrt{N_R(t)}e^{i\theta_R(t)}$, respectively, where $N_{L(R)}(t) \in \mathbb{R}$ represents the number of coherent magnons for each site in the left (right) FM and $\theta_{L(R)}(t) \in \mathbb{R}$ is the phase. Defining the relative phase as

$$\theta(t) = \theta_R(t) - \theta_L(t), \quad (\text{A2})$$

Eqs. (A1a) and (A1b) for $N_{L(R)}(t) \neq 0$ become

$$i\hbar\left(\frac{1}{2}\frac{\dot{N}_L}{N_L} + i\dot{\theta}_L\right) = \hbar(\Omega - i\gamma) + UN_L + \left[\mathcal{J}_{\text{Re}} + i\left(\mathcal{J}_{\text{Im}} - \frac{\hbar}{2}G\right)\right]\sqrt{\frac{N_R}{N_L}}e^{i\theta}, \quad (\text{A3a})$$

$$i\hbar\left(\frac{1}{2}\frac{\dot{N}_R}{N_R} + i\dot{\theta}_R\right) = \hbar(\Omega - i\gamma) + UN_R + \left[\mathcal{J}_{\text{Re}} - i\left(\mathcal{J}_{\text{Im}} + \frac{\hbar}{2}G\right)\right]\sqrt{\frac{N_L}{N_R}}e^{-i\theta}, \quad (\text{A3b})$$

where $\text{Re}(\mathcal{J}) = \mathcal{J}_{\text{Re}} \in \mathbb{R}$ and $\text{Im}(\mathcal{J}) = \mathcal{J}_{\text{Im}} \in \mathbb{R}$. Real and imaginary parts of Eqs. (A3a) and (A3b) provide

$$-\hbar\dot{\theta}_L = \hbar\Omega + UN_L + \left[\mathcal{J}_{\text{Re}} \cos \theta - \left(\mathcal{J}_{\text{Im}} - \frac{\hbar}{2}G\right) \sin \theta\right]\sqrt{\frac{N_R}{N_L}}, \quad (\text{A4a})$$

$$\frac{\hbar}{2}\frac{\dot{N}_L}{N_L} = -\hbar\gamma + \left[\mathcal{J}_{\text{Re}} \sin \theta + \left(\mathcal{J}_{\text{Im}} - \frac{\hbar}{2}G\right) \cos \theta\right]\sqrt{\frac{N_R}{N_L}}, \quad (\text{A4b})$$

$$-\hbar\dot{\theta}_R = \hbar\Omega + UN_R + \left[\mathcal{J}_{\text{Re}} \cos \theta - \left(\mathcal{J}_{\text{Im}} + \frac{\hbar}{2}G\right) \sin \theta\right]\sqrt{\frac{N_L}{N_R}}, \quad (\text{A4c})$$

$$\frac{\hbar}{2}\frac{\dot{N}_R}{N_R} = -\hbar\gamma - \left[\mathcal{J}_{\text{Re}} \sin \theta + \left(\mathcal{J}_{\text{Im}} + \frac{\hbar}{2}G\right) \cos \theta\right]\sqrt{\frac{N_L}{N_R}}, \quad (\text{A4d})$$

where Eq. (A4a) is the real part of Eq. (A3a), Eq. (A4b) is the imaginary part of Eq. (A3a), Eq. (A4c) is the real part of Eq. (A3b), and Eq. (A4d) is the imaginary part of Eq. (A3b). Taking the difference between Eqs. (A4a) and (A4c), those are rewritten as

$$\dot{\theta}(t) = \frac{\mathcal{J}_{\text{Re}}}{\hbar} \cos \theta \left(\sqrt{\frac{N_R}{N_L}} - \sqrt{\frac{N_L}{N_R}} \right) + \sin \theta \left[\left(\frac{\mathcal{J}_{\text{Im}}}{\hbar} + \frac{G}{2} \right) \sqrt{\frac{N_L}{N_R}} - \left(\frac{\mathcal{J}_{\text{Im}}}{\hbar} - \frac{G}{2} \right) \sqrt{\frac{N_R}{N_L}} \right] + u(N_L - N_R), \quad (\text{A5a})$$

$$\dot{N}_L(t) = -2\gamma N_L + 2 \left[\frac{\mathcal{J}_{\text{Re}}}{\hbar} \sin \theta + \left(\frac{\mathcal{J}_{\text{Im}}}{\hbar} - \frac{G}{2} \right) \cos \theta \right] \sqrt{N_L N_R}, \quad (\text{A5b})$$

$$\dot{N}_R(t) = -2\gamma N_R - 2 \left[\frac{\mathcal{J}_{\text{Re}}}{\hbar} \sin \theta + \left(\frac{\mathcal{J}_{\text{Im}}}{\hbar} + \frac{G}{2} \right) \cos \theta \right] \sqrt{N_L N_R}. \quad (\text{A5c})$$

In this study, we assume to continuously apply microwaves to each FM. The coherent magnon state, the key ingredient for the magnonic Josephson effect, is realized by microwave pumping. Under microwave pumping, coherent magnons are injected into each FM at the rate of \mathcal{P} [33]. Taking this effect of the magnon injection through microwave pumping into account, Eqs. (A5b) and (A5c) become

$$\dot{N}_L(t) = -2\gamma N_L + 2 \left[\frac{\mathcal{J}_{\text{Re}}}{\hbar} \sin \theta + \left(\frac{\mathcal{J}_{\text{Im}}}{\hbar} - \frac{G}{2} \right) \cos \theta \right] \sqrt{N_L N_R} + \mathcal{P}, \quad (\text{A6a})$$

$$\dot{N}_R(t) = -2\gamma N_R - 2 \left[\frac{\mathcal{J}_{\text{Re}}}{\hbar} \sin \theta + \left(\frac{\mathcal{J}_{\text{Im}}}{\hbar} + \frac{G}{2} \right) \cos \theta \right] \sqrt{N_L N_R} + \mathcal{P}. \quad (\text{A6b})$$

Finally, the magnonic Josephson equations under microwave pumping in the presence of non-local damping are summarized as

$$\dot{\theta}(t) = \frac{\mathcal{J}_{\text{Re}}}{\hbar} \cos \theta(t) \left(\sqrt{\frac{N_R(t)}{N_L(t)}} - \sqrt{\frac{N_L(t)}{N_R(t)}} \right) + \sin \theta(t) \left[\left(\frac{\mathcal{J}_{\text{Im}}}{\hbar} + \frac{G}{2} \right) \sqrt{\frac{N_L(t)}{N_R(t)}} - \left(\frac{\mathcal{J}_{\text{Im}}}{\hbar} - \frac{G}{2} \right) \sqrt{\frac{N_R(t)}{N_L(t)}} \right] + u[N_L(t) - N_R(t)], \quad (\text{A7a})$$

$$\dot{N}_L(t) = -2\gamma N_L(t) + 2 \left[\frac{\mathcal{J}_{\text{Re}}}{\hbar} \sin \theta(t) + \left(\frac{\mathcal{J}_{\text{Im}}}{\hbar} - \frac{G}{2} \right) \cos \theta(t) \right] \sqrt{N_L(t) N_R(t)} + \mathcal{P}, \quad (\text{A7b})$$

$$\dot{N}_R(t) = -2\gamma N_R(t) - 2 \left[\frac{\mathcal{J}_{\text{Re}}}{\hbar} \sin \theta(t) + \left(\frac{\mathcal{J}_{\text{Im}}}{\hbar} + \frac{G}{2} \right) \cos \theta(t) \right] \sqrt{N_L(t) N_R(t)} + \mathcal{P}. \quad (\text{A7c})$$

Appendix B: Nonequilibrium steady state for finite magnon interaction

In this Appendix, we provide details on the derivation of the equation for φ as a function of the magnon-magnon interaction. For

$$\mathcal{J}_{\text{Re}} = 0 \quad \text{and} \quad \mathcal{J}_{\text{Im}}/\hbar = G/2, \quad (\text{B1})$$

Eqs. (A7a)-(A7c) become

$$\dot{\theta}(t) = G \sqrt{\frac{N_L(t)}{N_R(t)}} \sin \theta(t) + u[N_L(t) - N_R(t)], \quad (\text{B2a})$$

$$\dot{N}_L(t) = -2\gamma N_L(t) + \mathcal{P}, \quad (\text{B2b})$$

$$\dot{N}_R(t) = -2\gamma N_R(t) - 2G \sqrt{N_L(t) N_R(t)} \cos \theta(t) + \mathcal{P}. \quad (\text{B2c})$$

Under microwave pumping \mathcal{P} , the nonequilibrium steady state $\dot{\theta}(t) = \dot{N}_L(t) = \dot{N}_R(t) = 0$ is realized, where $\theta(t)$, $N_L(t)$, and $N_R(t)$ approach asymptotically to time-independent constant as time advances, $\varphi = \lim_{t \rightarrow \infty} \theta(t)$ and $N_{L,R}^\infty = \lim_{t \rightarrow \infty} N_{L,R}(t)$. Thus, from Eqs. (B2a), (B2b) and (B2c), for $u \neq 0$, we get

$$N_L^\infty - N_R^\infty = -\frac{G}{u} \sqrt{\frac{N_L^\infty}{N_R^\infty}} \sin \varphi, \quad (\text{B3a})$$

$$N_L^\infty = \frac{\mathcal{P}}{2\gamma}, \quad (\text{B3b})$$

$$N_L^\infty - N_R^\infty = \frac{G}{\gamma} \sqrt{N_L^\infty N_R^\infty} \cos \varphi, \quad (\text{B3c})$$

From Eq. (B3c), we get the ratio between the number of coherent magnons in the left and right FMs,

$$\sqrt{\frac{N_R^\infty}{N_L^\infty}} = \sqrt{1 + \left(\frac{G}{2\gamma} \cos \varphi \right)^2} - \frac{G}{2\gamma} \cos \varphi. \quad (\text{B4})$$

Combining Eq. (B3a) and Eq. (B3c), we obtain

$$\tan \varphi = -\frac{u}{\gamma} N_R^\infty, \quad (\text{B5})$$

$$(N_L^\infty - N_R^\infty)^2 = -\frac{G^2}{\gamma u} N_L^\infty \frac{\sin(2\varphi)}{2}. \quad (\text{B6})$$

If $u > 0$, the solution exists only for $\tan \varphi < 0$. Substituting N_R^∞ from Eq. (B5) into Eq. (B6), we arrive at the implicit equation for $\tan \varphi$:

$$\left(\frac{\gamma}{u} \tan \varphi + N_L^\infty \right)^2 = -\frac{G^2}{\gamma u} N_L^\infty \frac{\tan \varphi}{1 + \tan^2 \varphi}. \quad (\text{B7})$$

This equation can be brought into the form of a quartic equation displayed in the main text:

$$\tan^4 \varphi + 2\tilde{u} \tan^3 \varphi + (1 + \tilde{u}^2) \tan^2 \varphi + \left[2 + \left(\frac{G}{\gamma} \right)^2 \right] \tilde{u} \tan \varphi + \tilde{u}^2 = 0, \quad (\text{B8})$$

where we introduced the rescaled dimensionless magnon-magnon interaction parameter $\tilde{u} = (u/\gamma) N_L^\infty$. We note that the solution is possible only for $\tan \varphi < 0$ ($\tan \varphi > 0$) for $u > 0$ ($u < 0$). We note that for a quartic polynomial one can find an explicit solution. However, it is too involved to be displayed here. In the main text we give the analytical expressions for φ for the limiting cases of small and large \tilde{u} .

Appendix C: Dynamics with different pumping rates

In this Appendix, we consider the case where $\mathcal{J}_{\text{Re}} = 0$, $\mathcal{J}_{\text{Im}}/\hbar = G/2$, and $u = 0$, with different pumping rates for two FMs. By solving the dynamics analytically, we show that our results do not rely on the initial conditions.

When we only pump the left FM with rate \mathcal{P} , the coupled dynamics is described by the following equations:

$$\begin{aligned}\dot{\theta} &= G\sqrt{\frac{N_L}{N_R}} \sin \theta, \\ \dot{N}_L &= -2\gamma N_L + \mathcal{P}, \\ \dot{N}_R &= -2\gamma N_R - 2G\sqrt{N_L N_R} \cos \theta.\end{aligned}\quad (\text{C1})$$

We now solve these equations analytically. We first introduce $n_{L/R}(t) = e^{2\gamma t} N_{L/R}(t)$, which allows us to rewrite the equations into the following form:

$$\dot{n}_L = e^{2\gamma t} \mathcal{P}, \quad \dot{\theta} = G\sqrt{\frac{n_L}{n_R}} \sin \theta, \quad \dot{n}_R = -2G\sqrt{n_R n_L} \cos \theta. \quad (\text{C2})$$

The first equation can be solved as

$$n_L(t) = N_L(0) + \frac{\mathcal{P}}{2\gamma}(e^{2\gamma t} - 1). \quad (\text{C3})$$

The last two equations leads to

$$\frac{d\theta}{dn_R} = -\frac{1 \tan \theta}{2 n_R} \quad (\text{C4})$$

and hence

$$|\sin \theta(t)|\sqrt{n_R(t)} = |\sin \theta(0)|\sqrt{N_R(0)}. \quad (\text{C5})$$

We then obtain the equation for $\theta(t)$ under the initial condition $\theta(0) \neq 0$ and $\theta(0) \neq \pm\pi$ as

$$\frac{d\theta}{dt} = \frac{G\sqrt{n_L(t)}}{|\sin \theta(0)|\sqrt{N_R(0)}} \sin \theta |\sin \theta|. \quad (\text{C6})$$

We remark that the above equation can be solved analytically because the integral of $\sqrt{n_L(t)}$ can be performed analytically. Henceforth, for our purpose, we focus on the case where $t \gg 1/(2\gamma)$ and hence $n_L(t) \approx (\mathcal{P}/2\gamma)e^{2\gamma t}$.

Here, without loss of generality, we consider the case of $\sin \theta(0) > 0$ and look for the solution that satisfies $\sin \theta(t) > 0$: One can similarly solve for the case when $\sin \theta(0) < 0$. We then get

$$\tan \theta(t) = \frac{1}{\cot \theta(0) - \alpha e^{\gamma t}} \quad (\text{C7})$$

and hence

$$\theta(t) = \arctan \left[\frac{1}{\cot \theta(0) - \alpha e^{\gamma t}} \right], \quad (\text{C8})$$

where α is the constant defined by

$$\alpha \equiv \frac{(G/\gamma)\sqrt{\mathcal{P}/(2\gamma)}}{\sin \theta(0)\sqrt{N_R(0)}}. \quad (\text{C9})$$

In the large $t \rightarrow \infty$ limit, we can drop $\cot \theta(0)$ in the expression. Then the expression of $\theta(t)$ is reduced to

$$\theta(t) = \pi - \frac{1}{\alpha} e^{-\gamma t}. \quad (\text{C10})$$

One can also easily write down the expression of $n_R(t)$ as

$$\sqrt{n_R(t)} = \alpha |\sin \theta(0)| \sqrt{N_R(0)} e^{2\gamma t}. \quad (\text{C11})$$

At large $t \rightarrow \infty$, we get

$$\sqrt{\frac{N_R^\infty}{N_L^\infty}} = \frac{G}{\gamma}. \quad (\text{C12})$$

It should be noted that this final value is independent of the initial condition and also the pumping rate \mathcal{P} .

When we pump the two FMs at the same time, the physics is very similar to the case that we discussed above. The only difference is that N_R^∞ is different. The equations are given by

$$\begin{aligned}\dot{\theta} &= G\sqrt{\frac{N_L}{N_R}} \sin \theta, \\ \dot{N}_L &= -2\gamma N_L + \mathcal{P}_L, \\ \dot{N}_R &= -2\gamma N_R - 2G\sqrt{N_L N_R} \cos \theta + \mathcal{P}_R,\end{aligned}\quad (\text{C13})$$

where \mathcal{P}_L and \mathcal{P}_R are the pumping rates of the two FMs. Introducing the ratio

$$\beta \equiv \sqrt{\frac{N_R^\infty}{N_L^\infty}}, \quad (\text{C14})$$

it is determined by the equation

$$\beta^2 - \frac{G}{\gamma}\beta - \frac{\mathcal{P}_R}{\mathcal{P}_L} = 0 \quad (\text{C15})$$

and hence

$$\beta = \frac{G/\gamma + \sqrt{(G/\gamma)^2 + 4\mathcal{P}_R/\mathcal{P}_L}}{2} \quad (\text{C16})$$

at $t \rightarrow \infty$. Here, without loss of generality, we consider the case of $\sin \theta(0) > 0$ and look for the solution that satisfies $\sin \theta(t) > 0$. Similar to our previous conclusion, $\theta(t)$ also approaches π exponentially fast but now with a different exponent as

$$\pi - \theta(t) \propto e^{-(G/\beta)t}. \quad (\text{C17})$$

We note that in the absence of the pumping of the right

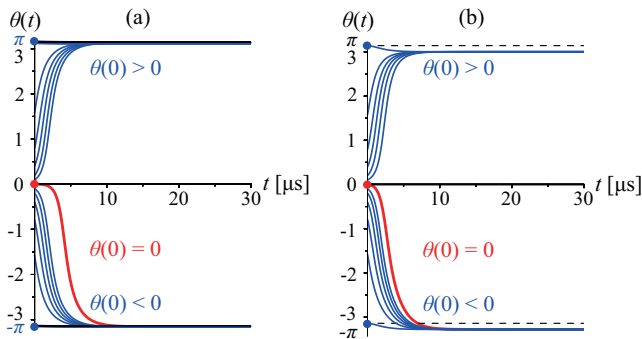


FIG. 4. Plots of the relative phase $\theta(t)$ as a function of time in the absence of the magnon-magnon interaction, i.e., $u = 0$, for the initial condition $\theta(0) = 0$ and $|\theta(0)| = \pi/2^n$ with $n = 0, 1, \dots, 5$ obtained by numerically solving Eqs. (A7a)-(A7c). The parameter values are the same as in Fig. 2 of the main text, e.g., $G = 1$ MHz, except for (a) $C_1 = C_2 = 10$ kHz and (b) $C_1 = 100$ kHz and $C_2 = 10$ kHz. Even in the presence of such perturbation $C_{1(2)}$, the synchronized precession of the left and the right magnetization, $\dot{\theta}(t) = 0$, remains valid, and the magnitude of φ is still bounded as Eq. (D2) where the value of φ slightly changes depending on the magnitude of the deviation (C_1 and C_2). Under the initial condition $\theta(0) = 0$, we get $\varphi \neq 0$ for $C_1 \neq 0$.

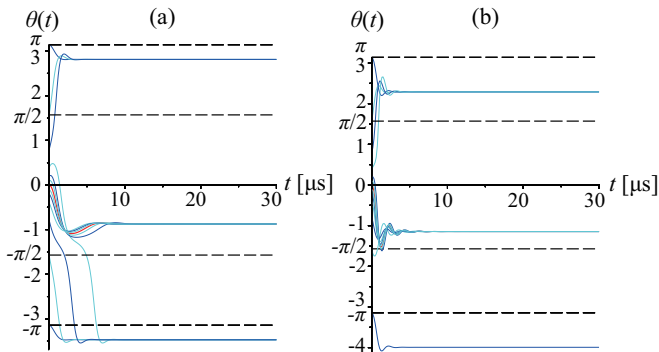


FIG. 5. Plots of the relative phase $\theta(t)$ as a function of time obtained by numerically solving Eqs. (A7a)-(A7c) for the same parameter values as in Fig. 4 except for (a) $C_1 = 1$ MHz and $C_2 = 10$ kHz and (b) $C_1 = C_2 = 1$ MHz. The magnitude of φ is no longer bounded as Eq. (D2), and the value of φ changes depending on the initial condition $\theta(0)$. Still, the synchronized precession of the left and the right magnetization, $\dot{\theta}(t) = 0$, remains valid. Under the initial condition $\theta(0) = 0$, we get $\varphi \neq 0$ for $C_1 \neq 0$.

FM $\mathcal{P}_R = 0$, we get $\beta = G/\gamma$ and $\pi - \theta(t) \propto e^{-\gamma t}$. This agrees with what we obtained before.

Appendix D: Robustness of synchronized precession

In the main text, to seek for the junction that exhibits a rectification effect characterized by $I_L(t) = 0$, we consider

the case

$$\mathcal{J}_{\text{Re}} = 0 \quad \text{and} \quad \mathcal{J}_{\text{Im}}/\hbar = G/2 > 0 \quad (\text{D1})$$

and find that the magnitude of φ is bounded as

$$\pi/2 < |\varphi| \leq \pi. \quad (\text{D2})$$

In this Appendix, although the rectification effect ceases to work and it becomes $I_L(t) \neq 0$, we numerically show that the synchronized precession of the left and the right magnetization, $\dot{\theta}(t) = 0$, remains valid even if the parameter values deviate from Eq. (D1). For this, we consider cases with

$$\mathcal{J}_{\text{Re}}/\hbar = C_1 \quad \text{and} \quad \mathcal{J}_{\text{Im}}/\hbar = G/2 + C_2, \quad (\text{D3})$$

where $C_{1(2)}$ is the constant that satisfies the condition $|\mathcal{J}| \ll \hbar\Omega$ for weakly spin-exchange coupled junctions. For $|C_1| \ll G$, Fig. 4 shows that the magnitude of φ is bounded as Eq. (D2). For $|C_1| \sim G$, i.e., when the value of C_1 increases and amounts to of the order of G , Fig. 5 shows that the magnitude of φ is no longer bounded as Eq. (D2). For $|C_2| \sim G$ and $C_1 = 0$, Fig. 6 shows that the value of φ differs from $\pm\pi$, but still its magnitude is bounded as Eq. (D2). We emphasize that the synchronized precession of the left and the right magnetization, $\dot{\theta}(t) = 0$, remains valid in all of these cases (Figs. 4-6). We also note that under the initial condition $\theta(0) = 0$, Figs. 4-6 with Fig. 2 of the main text show that we get $\varphi \neq 0$ for $C_1 \neq 0$, whereas $\varphi = 0$ for $C_1 = 0$. Also in this sense, the point $\theta(0) = 0$ is instable.

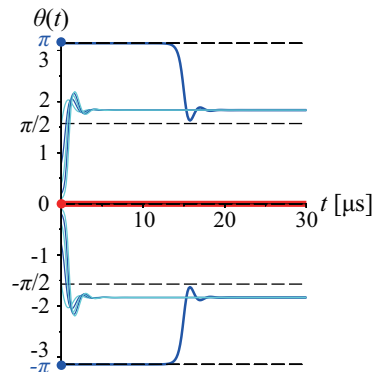


FIG. 6. Plots of the relative phase $\theta(t)$ as a function of time obtained by numerically solving Eqs. (A7a)-(A7c) for the same parameter values as in Fig. 5 except for $C_1 = 0$ and $C_2 = 1$ MHz. The magnitude of φ is bounded as Eq. (D2), and the synchronized precession of the left and the right magnetization, $\dot{\theta}(t) = 0$, remains valid. Under the initial condition $\theta(0) = 0$, we get $\varphi = 0$ for $C_1 = 0$.

- [1] Y. Ashida, Z. Gong, and M. Ueda, “Non-Hermitian physics,” *Adv. Phys.* **69**, 249 (2020), [arXiv:2006.01837](#).
- [2] A. V. Chumak, V. I. Vasyuchka, A. A. Serga, and B. Hillebrands, “Magnon spintronics,” *Nat. Phys.* **11**, 453 (2015).
- [3] A. V. Chumak, P. Kabos, M. Wu, C. Abert, C. Adelman, A. Adeyeye, J. Åkerman, F. G. Aliev, A. Anane, A. Awad, *et al.*, “Advances in magnetism roadmap on spin-wave computing,” *IEEE Trans. Magn.* **58**, 1 (2022), [arXiv:2111.00365](#).
- [4] H. Yuan, Y. Cao, A. Kamra, R. A. Duine, and P. Yan, “Quantum magnonics: when magnon spintronics meets quantum information science,” *Phys. Rep.* **965**, 1 (2022), [arXiv:2111.14241](#).
- [5] K. Nakata, K. A. van Hoogdalem, P. Simon, and D. Loss, “Josephson and persistent spin currents in Bose-Einstein condensates of magnons,” *Phys. Rev. B* **90**, 144419 (2014), [arXiv:1406.7004](#).
- [6] R. E. Troncoso and Á. S. Núñez, “Josephson effects in a Bose-Einstein condensate of magnons,” *Ann. Phys. (N. Y.)* **346**, 182 (2014), [arXiv:1305.4285](#).
- [7] Y. Liu, G. Yin, J. Zang, R. K. Lake, and Y. Barlas, “Spin-Josephson effects in exchange coupled antiferromagnetic insulators,” *Phys. Rev. B* **94**, 094434 (2016), [arXiv:1605.09427](#).
- [8] R. Khymyn, I. Lisenkov, V. Tiberkevich, B. A. Ivanov, and A. Slavin, “Antiferromagnetic THz-frequency Josephson-like oscillator driven by spin current,” *Sci. Rep.* **7**, 43705 (2017), [arXiv:1609.09866](#).
- [9] T. Yu, J. Zou, B. Zeng, J. Rao, and K. Xia, “Non-Hermitian topological magnonics,” *Phys. Rep.* **1062**, 1 (2024), [arXiv:2306.04348](#).
- [10] Y. Tserkovnyak, “Exceptional points in dissipatively coupled spin dynamics,” *Phys. Rev. Res.* **2**, 013031 (2020), [arXiv:1911.01619](#).
- [11] J. Zou, S. Bosco, E. Thingstad, J. Klinovaja, and D. Loss, “Dissipative spin-wave diode and nonreciprocal magnonic amplifier,” *Phys. Rev. Lett.* **132**, 036701 (2024), [arXiv:2306.15916](#).
- [12] L. Bulaevskii, V. Kuzii, and A. Sobyenin, “Superconducting system with weak coupling to the current in the ground state,” *J. Exp. Theor. Phys. Lett.* **25**, 290 (1977).
- [13] V. B. Geshkenbein, A. I. Larkin, and A. Barone, “Vortices with half magnetic flux quanta in “heavy-fermion” superconductors,” *Phys. Rev. B* **36**, 235 (1987).
- [14] M. Sigrist and T. M. Rice, “Paramagnetic effect in high T_c superconductors—a hint for d -wave superconductivity,” *J. Phys. Soc. Jpn.* **61**, 4283 (1992).
- [15] D. A. Wollman, D. J. Van Harlingen, W. C. Lee, D. M. Ginsberg, and A. J. Leggett, “Experimental determination of the superconducting pairing state in YBCO from the phase coherence of YBCO-Pb dc SQUIDs,” *Phys. Rev. Lett.* **71**, 2134 (1993).
- [16] D. J. Van Harlingen, “Phase-sensitive tests of the symmetry of the pairing state in the high-temperature superconductors—Evidence for $d_{x^2-y^2}$ symmetry,” *Rev. Mod. Phys.* **67**, 515 (1995).
- [17] V. V. Ryazanov, V. A. Oboznov, A. Yu. Rusanov, A. V. Veretennikov, A. A. Golubov, and J. Aarts, “Coupling of two superconductors through a ferromagnet: Evidence for a π junction,” *Phys. Rev. Lett.* **86**, 2427 (2001), [arXiv:cond-mat/0008364](#).
- [18] E. Il’ichev, M. Grajcar, R. Hlubina, R. P. J. IJsselsteijn, H. E. Hoening, H.-G. Meyer, A. Golubov, M. H. S. Amin, A. M. Zagorskin, A. N. Omelyanchouk, and M. Yu. Kupriyanov, “Degenerate ground state in a mesoscopic $\text{YBa}_2\text{Cu}_3\text{O}_{7-x}$ grain boundary Josephson junction,” *Phys. Rev. Lett.* **86**, 5369 (2001), [arXiv:cond-mat/0102404](#).
- [19] G. Testa, A. Monaco, E. Esposito, E. Sarnelli, D.-J. Kang, S. Mennema, E. Tarte, and M. Blamire, “Midgap state-based π -junctions for digital applications,” *Appl. Phys. Lett.* **85**, 1202 (2004).
- [20] H. Sickinger, A. Lipman, M. Weides, R. G. Mints, H. Kohlstedt, D. Koelle, R. Kleiner, and E. Goldobin, “Experimental evidence of a φ Josephson junction,” *Phys. Rev. Lett.* **109**, 107002 (2012), [arXiv:1207.3013](#).
- [21] E. Goldobin, H. Sickinger, M. Weides, N. Ruppelt, H. Kohlstedt, R. Kleiner, and D. Koelle, “Memory cell based on a φ Josephson junction,” *Appl. Phys. Lett.* **102**, 242602 (2013), [arXiv:1306.1683](#).
- [22] D. Szombati, S. Nadj-Perge, D. Car, S. Plissard, E. Bakkers, and L. Kouwenhoven, “Josephson φ_0 -junction in nanowire quantum dots,” *Nat. Phys.* **12**, 568 (2016), [arXiv:1512.01234](#).
- [23] Y. Tanaka and S. Kashiwaya, “Theory of the Josephson effect in d -wave superconductors,” *Phys. Rev. B* **53**, R11957 (1996).
- [24] Y. S. Barash, H. Burkhardt, and D. Rainer, “Low-temperature anomaly in the Josephson critical current of junctions in d -wave superconductors,” *Phys. Rev. Lett.* **77**, 4070 (1996).
- [25] Y. Tanaka and S. Kashiwaya, “Theory of Josephson effects in anisotropic superconductors,” *Phys. Rev. B* **56**, 892 (1997).
- [26] R. G. Mints, “Self-generated flux in Josephson junctions with alternating critical current density,” *Phys. Rev. B* **57**, R3221 (1998).
- [27] R. G. Mints and I. Papiashvili, “Josephson vortices with fractional flux quanta at $\text{YBa}_2\text{Cu}_3\text{O}_{7-x}$ grain boundaries,” *Phys. Rev. B* **64**, 134501 (2001), [arXiv:cond-mat/0101085](#).
- [28] A. Buzdin and A. E. Koshelev, “Periodic alternating 0- and π -junction structures as realization of φ -Josephson junctions,” *Phys. Rev. B* **67**, 220504 (2003), [arXiv:cond-mat/0305142](#).
- [29] A. Gumann, C. Iniotakis, and N. Schopohl, “Geometric π Josephson junction in d -wave superconducting thin films,” *Appl. Phys. Lett.* **91**, 192502 (2007), [arXiv:0708.3898](#).
- [30] A. Buzdin, “Direct coupling between magnetism and superconducting current in the Josephson φ_0 junction,” *Phys. Rev. Lett.* **101**, 107005 (2008), [arXiv:0808.0299](#).
- [31] E. Goldobin, D. Koelle, R. Kleiner, and R. G. Mints, “Josephson junction with a magnetic-field tunable ground state,” *Phys. Rev. Lett.* **107**, 227001 (2011), [arXiv:1110.2326](#).
- [32] See Ref. [64] for observation of anomalous Josephson effect in metallic and nonmagnetic superconducting-normal-superconducting junctions configured as nonequilibrium Andreev interferometers [65–67].
- [33] K. Nakata, P. Simon, and D. Loss, “Magnon transport

- through microwave pumping,” *Phys. Rev. B* **92**, 014422 (2015), [arXiv:1502.03865](#).
- [34] T. Holstein and H. Primakoff, “Field dependence of the intrinsic domain magnetization of a ferromagnet,” *Phys. Rev.* **58**, 1098 (1940).
- [35] F. Meier and D. Loss, “Magnetization transport and quantized spin conductance,” *Phys. Rev. Lett.* **90**, 167204 (2003), [arXiv:cond-mat/0209521](#).
- [36] R. O. Serha, V. I. Vasyuchka, A. A. Serga, and B. Hillebrands, “Towards an experimental proof of the magnonic Aharonov-Casher effect,” *Phys. Rev. B* **108**, L220404 (2023), [arXiv:2312.05113](#).
- [37] H. Katsura, N. Nagaosa, and A. V. Balatsky, “Spin current and magnetoelectric effect in non-collinear magnets,” *Phys. Rev. Lett.* **95**, 057205 (2005), [arXiv:cond-mat/0412319](#).
- [38] S. Liang, R. Chen, Q. Cui, Y. Zhou, F. Pan, H. Yang, and C. Song, “Ruderman–Kittel–Kasuya–Yosida-type interlayer Dzyaloshinskii–Moriya interaction in synthetic magnets,” *Nano Lett.* **23**, 8690 (2023).
- [39] F. Kammerbauer, W.-Y. Choi, F. Freimuth, K. Lee, R. Frömter, D.-S. Han, R. Lavrijsen, H. J. Swagten, Y. Mokrousov, and M. Kläui, “Controlling the interlayer Dzyaloshinskii–Moriya interaction by electrical currents,” *Nano Lett.* **23**, 7070 (2023).
- [40] B. Heinrich, Y. Tserkovnyak, G. Woltersdorf, A. Brataas, R. Urban, and G. E. W. Bauer, “Dynamic exchange coupling in magnetic bilayers,” *Phys. Rev. Lett.* **90**, 187601 (2003), [arXiv:cond-mat/0210588](#).
- [41] J. Zou, S. Zhang, and Y. Tserkovnyak, “Bell-state generation for spin qubits via dissipative coupling,” *Phys. Rev. B* **106**, L180406 (2022), [arXiv:2108.07365](#).
- [42] J. Zou, S. Bosco, and D. Loss, “Spatially correlated classical and quantum noise in driven qubits,” *npj Quantum Inf.* **10**, 46 (2024), [arXiv:2308.03054](#).
- [43] See the Appendix A for the derivation of the magnonic Josephson equations, the Appendix B for the derivation of the equation for φ as a function of the magnon-magnon interaction, the Appendix C for spin dynamics with different pumping rates, and the Appendix D for the parameter dependence of our results.
- [44] B. D. Josephson, “Possible new effects in superconductive tunnelling,” *Phys. Lett.* **1**, 251 (1962).
- [45] K. Nakata, P. Simon, and D. Loss, “Wiedemann-Franz law for magnon transport,” *Phys. Rev. B* **92**, 134425 (2015), [arXiv:1507.03807](#).
- [46] K. Nakata, P. Simon, and D. Loss, “Spin currents and magnon dynamics in insulating magnets,” *J. Phys. D: Appl. Phys.* **50**, 114004 (2017), [arXiv:1610.08901](#).
- [47] Y. Zhang, Y. Gu, P. Li, J. Hu, and K. Jiang, “General theory of Josephson diodes,” *Phys. Rev. X* **12**, 041013 (2022), [arXiv:2112.08901](#).
- [48] M. Davydova, S. Prembabu, and L. Fu, “Universal Josephson diode effect,” *Sci. Adv.* **8**, eabo0309 (2022), [arXiv:2201.00831](#).
- [49] H. Wu, Y. Wang, Y. Xu, P. K. Sivakumar, C. Pasco, U. Filippozzi, S. S. P. Parkin, Y.-J. Zeng, T. McQueen, and M. N. Ali, “The field-free Josephson diode in a van der Waals heterostructure,” *Nature* **604**, 653 (2022), [arXiv:2103.15809](#).
- [50] S. S. P. Parkin, N. More, and K. P. Roche, “Oscillations in exchange coupling and magnetoresistance in metallic superlattice structures: Co/Ru, Co/Cr, and Fe/Cr,” *Phys. Rev. Lett.* **64**, 2304 (1990).
- [51] S. S. P. Parkin, R. Bhadra, and K. P. Roche, “Oscillatory magnetic exchange coupling through thin copper layers,” *Phys. Rev. Lett.* **66**, 2152 (1991).
- [52] S. Husain, S. Pal, X. Chen, P. Kumar, A. Kumar, A. K. Mondal, N. Behera, N. K. Gupta, S. Hait, R. Gupta, R. Brucas, B. Sanyal, A. Barman, S. Chaudhary, and P. Svedlindh, “Large Dzyaloshinskii–Moriya interaction and atomic layer thickness dependence in a ferromagnet-WS₂ heterostructure,” *Phys. Rev. B* **105**, 064422 (2022).
- [53] J. Yun, B. Cui, Q. Cui, X. He, Y. Chang, Y. Zhu, Z. Yan, X. Guo, H. Xie, J. Zhang, *et al.*, “Anisotropic interlayer Dzyaloshinskii–Moriya interaction in synthetic ferromagnetic/antiferromagnetic sandwiches,” *Adv. Funct. Mater.* **2301731** (2023).
- [54] T. Srivastava, M. Schott, R. Juge, V. Krizakova, M. Belmeguenai, Y. Roussigné, A. Bernard-Mantel, L. Ranno, S. Pizzini, S.-M. Chérif, *et al.*, “Large-voltage tuning of Dzyaloshinskii–Moriya interactions: A route toward dynamic control of skyrmion chirality,” *Nano Lett.* **18**, 4871 (2018).
- [55] C.-E. Fillion, J. Fischer, R. Kumar, A. Fassatoui, S. Pizzini, L. Ranno, D. Ourdani, M. Belmeguenai, Y. Roussigné, S.-M. Chérif, *et al.*, “Gate-controlled skyrmion and domain wall chirality,” *Nat. Commun.* **13**, 5257 (2022), [arXiv:2204.04031](#).
- [56] T. Koyama, Y. Nakatani, J. Ieda, and D. Chiba, “Electric field control of magnetic domain wall motion via modulation of the Dzyaloshinskii–Moriya interaction,” *Sci. Adv.* **4**, eaav0265 (2018).
- [57] E. Y. Vedmedenko, P. Riego, J. A. Arregi, and A. Berger, “Interlayer Dzyaloshinskii–Moriya interactions,” *Phys. Rev. Lett.* **122**, 257202 (2019), [arXiv:1803.10570](#).
- [58] L. J. Cornelissen, J. Liu, R. A. Duine, J. B. Youssef, and B. J. v. Wees, “Long-distance transport of magnon spin information in a magnetic insulator at room temperature,” *Nat. Phys.* **11**, 1022 (2015), [arXiv:1505.06325](#).
- [59] P. N. Boltyk, O. Dzyapko, V. E. Demidov, N. G. Berloff, and S. O. Demokritov, “Spatially non-uniform ground state and quantized vortices in a two-component Bose-Einstein condensate of magnons,” *Sci. Rep.* **2**, 482 (2012).
- [60] P. Pirro, V. I. Vasyuchka, A. A. Serga, and B. Hillebrands, “Advances in coherent magnonics,” *Nat. Rev. Mater.* **6**, 1114 (2021).
- [61] A. J. E. Kreil, H. Y. M. Shmarova, P. Frey, A. Pomyalov, V. S. L’vov, G. A. Melkov, A. A. Serga, and B. Hillebrands, “Experimental observation of Josephson oscillations in a room-temperature Bose-Einstein magnon condensate,” *Phys. Rev. B* **104**, 144414 (2021), [arXiv:1911.07802](#).
- [62] D. A. Bozhko, A. A. Serga, P. Clausen, V. I. Vasyuchka, F. Heussner, G. A. Melkov, A. Pomyalov, V. S. L’vov, and B. Hillebrands, “Supercurrent in a room-temperature Bose-Einstein magnon condensate,” *Nat. Phys.* **12**, 1057 (2016), [arXiv:1503.00482](#).
- [63] B. Heinrich, C. Burrowes, E. Montoya, B. Kardasz, E. Girt, Y. Y. Song, Y. Sun, and M. Wu, “Spin pumping at the magnetic insulator (YIG)/normal metal (Au) interfaces,” *Phys. Rev. Lett.* **107**, 066604 (2011).
- [64] D. Margineda, J. S. Claydon, F. Qejvanaj, and C. Checkley, “Observation of anomalous Josephson effect in nonequilibrium Andreev interferometers,” *Phys. Rev. B* **107**, L100502 (2023), [arXiv:2105.13968](#).
- [65] P. E. Dolgirev, M. S. Kalenkov, and A. D. Zaikin, “Interplay between Josephson and Aharonov-Bohm effects

- in Andreev interferometers,” *Sci. Rep.* **9**, 1301 (2019), [arXiv:1807.10339](#).
- [66] P. E. Dolgirev, M. S. Kalenkov, A. E. Tarkhov, and A. D. Zaikin, “Phase-coherent electron transport in asymmetric crosslike Andreev interferometers,” *Phys. Rev. B* **100**, 054511 (2019), [arXiv:1906.07305](#).
- [67] A. Hijano, S. Ilić, and F. S. Bergeret, “Anomalous Andreev interferometer: Study of an anomalous Josephson junction coupled to a normal wire,” *Phys. Rev. B* **104**, 214515 (2021), [arXiv:2106.14021](#).